On the orthotropic elasto-plastic material response of additively manufactured polyamide 12

N. Lammens[1,2], I. De Baere[1,3] & W. Van Paepegem[1]
[1] *Ghent University, Zwijnaarde, Belgium*
[2] *SIM vzw., STREAM, Zwijnaarde, Belgium*
[3] *SIM vzw., M3-AMCAE, Zwijnaarde, Belgium*

ABSTRACT: The mechanical response of polymers such as polyamide 12 (PA-12) manufactured through additive manufacturing, is significantly affected by the layered manufacturing approach and the printer settings used during the creation of the parts. As a result, the mechanical performance can differ significantly from PA-12 parts created through conventional techniques such as injection molding, and a detailed study of the material mechanical behavior is necessary. This work presents an in-depth study of the response of PA-12 to tensile loading and the challenges involved in obtaining qualitative and repeatable results. The full elasto-plastic curves are measured during tensile testing and the effect of printing direction is taken into account in order to investigate whether orthotropic material behavior can be observed. All parts were manufactured using commercially available selective laser sintering (SLS) printers. Digital image correlation was used extensively to obtain high-accuracy strain measurement over the entire elasto-plastic range up to failure. The results show an isotropic elastic response of PA-12, with orthotropic failure properties and the presence of significant viscous contributions in the material response.

1 INTRODUCTION

Keywords such as 3D printing, additive manufacturing, rapid prototyping,… have received a large amount of interest during the last decade as a potentially revolutionizing technology. The layered manufacturing technique associated with these production methods, enables the production of intricate geometries which cannot be achieved with traditional manufacturing techniques, without the need for specialized tooling. Over the past years, several techniques such as fused deposition manufacturing (FDM), stereo-lithography (SLA) and laser sintering (SLS) have emerged as mature techniques within the 3D printing industry.

While the original application of 3D printing was focused on rapid prototyping applications, placing no requirements on mechanical properties, the improvements in process control and raw material properties have opened up the possibility of rapid manufacturing and rapid tooling of structural (load carrying) parts.

In order to ensure the proper and safe use of these 3D printed parts, a good understanding of the mechanical characteristics of the material and manufacturing technique is inevitable. Several factors, including the layered build-up, scanning pattern, lack of over-pressure during manufacturing, specific thermal history during manufacturing, post-processing,… can potentially affect the material response compared to the characteristics obtained using traditional manufacturing techniques (Zarringhalam, Hopkinson et al. 2006, Starr, Gornet et al. 2011, Goodridge, Tuck et al. 2012). For example, the layered manufacturing approach has led to research on possible orthotropic material response of laser sintered parts (Ajoku, Saleh et al. 2006, Cooke, Tomlinson et al. 2011, Shaffer, Yang et al. 2014). Others have investigated the fatigue response of laser sintered PA-12 (Van Hooreweder, Moens et al. 2013, Munguia and Dalgarno 2014, Salazar, Rico et al. 2014). In order to properly design 3D printed structures which have to provide a load-carrying ability, a proper and full understanding of the mechanical response is necessary.

In this work, the mechanical behavior of laser sintered PA-12 is investigated experimentally, as it represents a cost-effective material for several applications. The full elasto-plastic material response is investigated. The effect of printing orientation on the mechanical response is investigated to assess whether directionally-dependent material properties can be observed (i.e. true material orthotropy) or whether observed variations in mechanical properties are only dependent on the location within the build volume (absolute to the volume and relative to neighboring samples). Special attention is given to the challenges involved in obtaining highly accurate and repeatable measurement data.

2 SAMPLE DESCRIPTION

2.1 *Sample description*

All samples were manufactured on a commercial SLS machine at Materialise, Belgium. All the samples were produced using a P395 machine from EOS GmbH using a PA2200 PA12 powder with a mixing ratio 50/50 between virgin and recycled powder and an alternate x–y scanning pattern, using an energy density of 33J/mm². All samples were printed within a single, dedicated batch and detailed information on the position of all samples within the batch was made available allowing us to assess whether observed differences can be attributed solely to material orthotropy, or also a result of the location within the build volume.

The samples have a dogbone geometry, in accordance with the ASTM D638 standard. The sample have a nominal length of 246mm, a gauge width of 19mm and thickness of 7mm. Samples were printed with 3 different orientations relative to the print-bed: flatwise, edgewise and upright as shown in Figure 1.

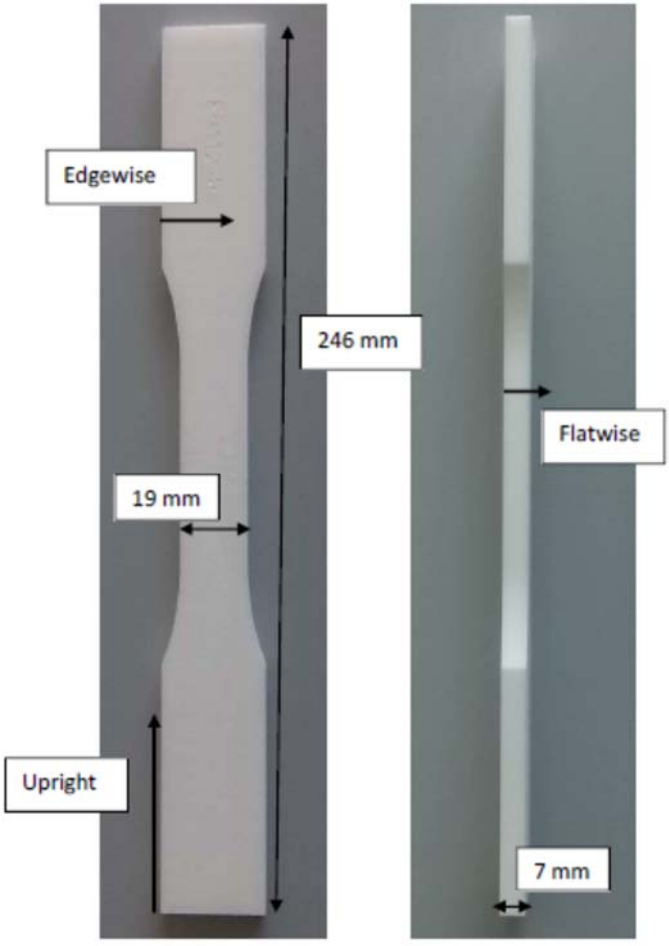

Figure 1. Dogbone sample dimensions, geometry and designation

All samples are tested in the as-printed condition, and no subsequent post-processing was applied.

2.2 *Test equipment*

All tests were performed on a hydraulic INSTRON 8801 tensile machine. The machine is equipped with a special alignment kit, allowing to accurately align both grips in order to avoid any measurement-errors induced by torsion, bending and/or misalignment of the sample during tensile testing. The alignment of the machine was confirmed using a dedicated alignment tool and through digital image correlation (DIC) results.

By default, an extensometer with a 4% strain range was used to measure elongation of the samples. As these extensometers do not allow to measure large strains or failure, the tensile tests are briefly interrupted at 1% strain to remove the extensometer before continuing up to failure. In addition to the extensometer, 3D DIC was used to measure the complete strain response of the samples. Two Allied Vision Stingray 2MP cameras with a framerate of 2Hz were used. In order to properly capture the full stress-strain curve using DIC, the displacement rate of the tensile machine was limited to 2mm/min (rather than the advised 5mm/min within ASTM D638).

3 RESULTS

3.1 *Tensile tests*

A total of 4 edgewise, 4 flatwise and 4 upright samples were used to perform tensile tests up to failure. Figure 2 shows the resulting stress-strain curves for an edgewise (E9112/7), flatwise (F9112/56) and upright (U9112/86) sample obtained using DIC strain data. The first letter in the label refers to the printing direction (E = edgewise, F = flatwise, U = upright), the four digit code identifies the unique build (9112) and the digits trailing the '/' symbol, identify the part in the build. The shown curves are representative for all tests performed, and very little scatter was observed between different samples of the same build-orientation.

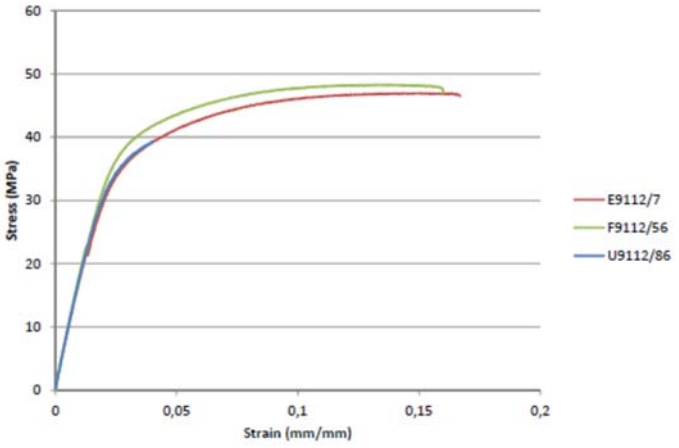

Figure 2. Stress-strain curves for different print-orientations

Already, Figure 2 indicates a difference in mechanical response depending on the print orientation.

3.1.1 *Stiffness*

In order to determine the stiffness (Young's modulus) of the different samples, both extensometer data and 3D DIC data is available. Figure 3 shows a close-up of the derived stiffness within the 0 – 0.2% strain range using strain data from the extensometer, compared to strain data from 3D DIC measurements.

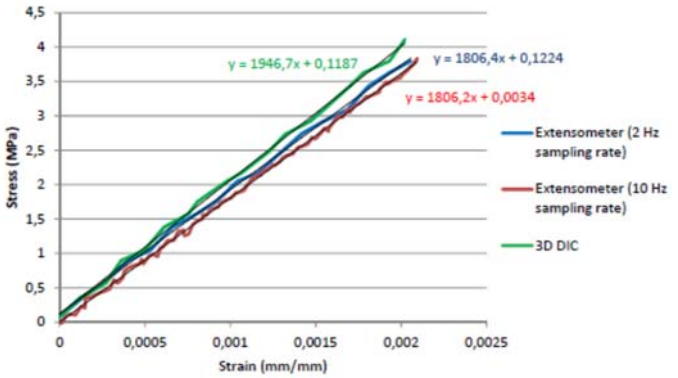

Figure 3. Determination of stiffness based on extensometer and DIC data for the edgewise E9112/7 sample

Minimal differences are observed when changing the sampling rate of the extensometer (2 Hz vs. 10 Hz), showing that DIC sampling at 2 Hz is sufficient to determine the Young's modulus. However, a significant difference in obtained stiffness (1806 MPa vs. 1947 MPa) can be observed, with the lower stiffness obtained using extensometer data.

Extensive testing has revealed that extensometer data result in large variations in derived Young's moduli, both over- and underestimating stiffness compared to 3D DIC data. Figure 4 gives an overview of the derived Young's moduli for all samples tested, using extensometer (blue) and 3D DIC (green) data.

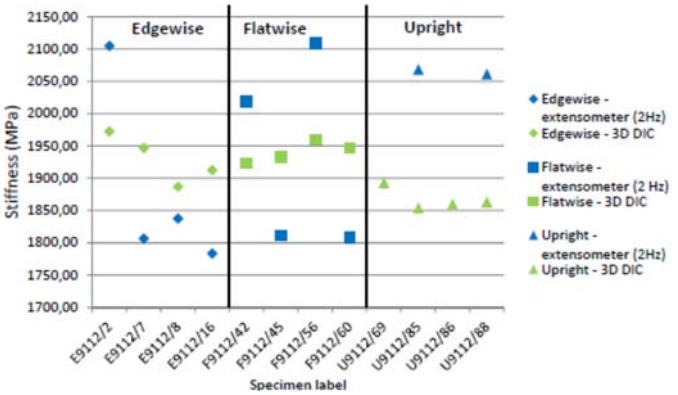

Figure 4. Variations in Young's modulus using extensometer (blue) and DIC (green) strain data

Clearly, using extensometer readings results in unacceptable variations in stiffness, which do no correlate to observations using DIC, and are therefore expected to be a result of measurement errors, rather than a consequence of sample variability.

It is believed that extensometer alignment, indentation into the soft PA-12 surface and the rough surface of the samples all contribute to the variations observed in the extensometer data. As a result, only strain data obtained through 3D DIC will be used as a reliable strain measurement.

Additionally, while Figure 2 suggests an initial linear region in the stress-strain curve, it was found that even for low strains the PA-12 behavior is not linear but rather quadratic, and therefore stiffness derivation is strongly dependent on the precise strain range used. Variations of up to 100MPa (or 5%) could be obtained by extending or reducing the strain range used to derive the stiffness. Unfortunately, ASTM D638 does not provide a fixed strain range for stiffness derivation, which may result in different Young's moduli between different researchers. Clearly, for the purpose of these tests all Young's moduli are derived using a fixed strain range of 0 – 0.2% (Engineering) strain.

Considering that all samples were printed closely to each other, and using this strain range, the Young's modulus can be seen to be isotropic (i.e. independent of print orientation) and close to 1900MPa.

3.1.2 *Poisson's ratio*

Another benefit of using DIC, is the fact that it records the full strain field rather than a single strain value. As such it can be used to extract the Poisson's ratio during tensile testing. The averaged Poisson's ratios for different orientations are given in Table 1.

Table 1. Poisson's ratio for different printing orientations

	Poisson's ratio
Edgewise	0.39
Flatwise	0.42
Upright	0.41

The values shown above indicate a Poisson's ratio between 0.39 and 0.42. These values correspond with data obtained through ultrasonic, non-destructive measurements where a Poisson's ratio between 0.38 and 0.41 was measured. This also corresponds to data found in literature (Ramos-Grez, Amado-Becker et al. 2008). It should be noted that the accuracy in Poisson's ratio determination through DIC is insufficient to clearly determine whether all Poisson coefficients are identical, or whether a difference exists between the three printing orientations. Non-destructive, ultrasonic tests rely on time-of-flight measurements of an ultrasonic wave through the sample (related to sample stiffness). Therefore, accuracy of ultrasonic tests are not (significantly) dependent on applied strain levels, but rather determined by the accuracy of time-of-flight measurements. As such, using proper equipment, higher accuracies can be obtained in Poisson's ratio determination than through DIC analysis of tensile testing. The ultrasonic results, which were performed in current study suggest a distinction between upright printed samples on the one hand, and flatwise and edgewise samples on the other hand. However,

these differences are minimal and can be ignored for most applications.

3.1.3 *Ultimate tensile strength*

Figure 2 already suggested differences in ultimate tensile strength when comparing upright samples to flatwise and edgewise samples. Figure 5 shows the UTS values obtained for all samples tested within this work.

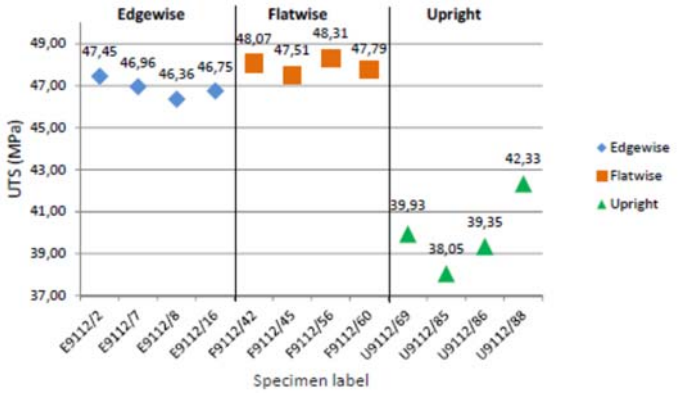

Figure 5. Ultimate tensile strength for different print orientations

Clearly, the upright samples are significantly weaker than the edgewise and flatwise samples. This behavior is an obvious consequence of the layered manufacturing approach. Within a single layer of material, subsequent scan lines are fused together tightly as the different lines are not given sufficient time to cool down before they are fused together. However, the elapsed time between application of two subsequent layers is sufficient to allow for some degree of solidification of the bottom layer, resulting in a less profound fusion between the subsequent layers. As a result, the tensile strength is lower between different layers (i.e. in upright samples) as between different scan lines (i.e. flatwise and edgewise samples).
In addition, µCT scanning techniques reveal that porosities included within the material, are localized between the different layers and will have an effect on the total strength of the sample in that direction (i.e. the upright print direction).

3.1.4 *Failure strain*

Similar to the observations for UTS, Figure 2 shows a clear difference in failure strain between upright, edgewise and flatwise samples. Figure 6 shows the failure strains obtained for the different printing orientations tested.

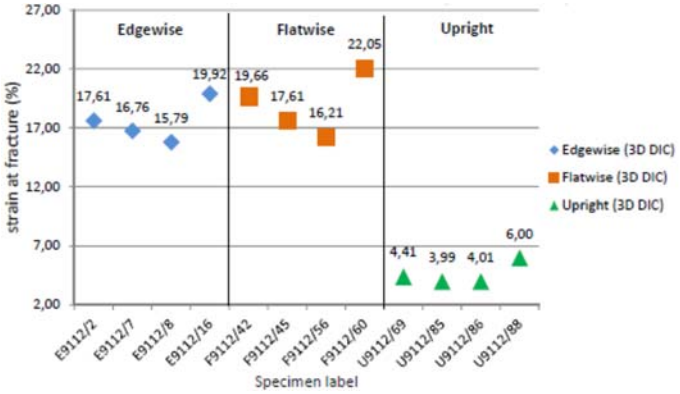

Figure 6. Failure strains for different print orientations

Both edgewise and flatwise samples have failure strains around 20%, while the upright samples fail at a much lower strain of approximately 5%. Again, this behavior can be attributed to the different bond strength obtained within a single layer as compared to between individual printing layers.
Consequently, while stiffness and Poisson ratio can be considered to be nearly isotropic for the material and conditions tested, the UTS and failure strain cannot be modeled as isotropic, and anisotropic failure properties need to be taken into account to properly design structures using this material and method.

3.1.5 *Hysteresis tests*

As stated previously, the extensometer used has a strain range up to 4% strain and cannot withstand the energy release associated with sample failure. As a result, the tensile tests were interrupted at strain levels near 1% in order to safely remove the extensometer before continuing the tests to rupture. Figure 7 shows the resulting relaxation occurring during this event.

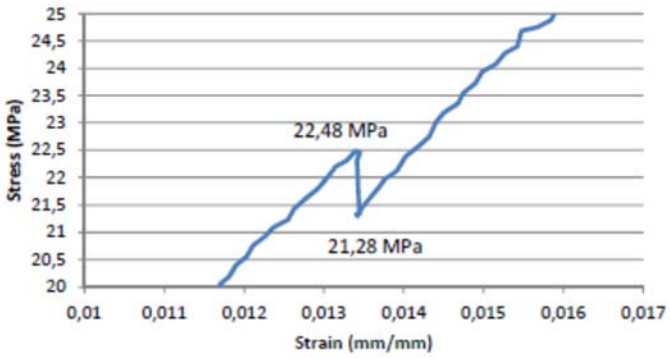

Figure 7. Stress relaxation during removal of extensometer

Clear relaxation can be observed even though the interruption of the test was on the order of seconds. This phenomenon is indicative of the visco-elastic material response of PA-12 rather than pure elastic material behavior.
In order to get a first indication of the viscous contributions in polyamide, a couple of preliminary hysteresis tests were performed in which several load-unload cycles were performed to a constant stress level. Repetitive cyclic loading was applied to different constant stress levels to assess the hysteretic energy loss and the occurrence of damage. Stress levels were

chosen at 25 MPa (elastic region), 35 MPa (transition between elastic and plastic) and 45 MPa (plastic region). All tests were performed at a fixed displacement rate of 2mm/min in order to obtain sufficient DIC data during the test. Figure 8 shows the stress-strain curve for repetitive loading of an edgewise sample up to 45MPa.

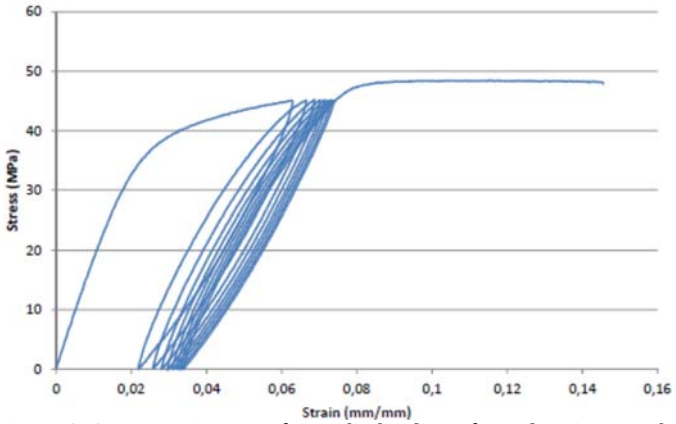

Figure 8. Stress-strain curve for cyclic loading of an edgewise sample to 45MPa

The results indicate that the hysteresis loop stabilizes after just a couple of cycles, indicating no further damage is induced in the samples. Consequently, the energy loss can be considered to be attributed to the viscous nature of the polymer.
Combined with the previous static material data, these curves can be used to derive the viscous nature of 3D printed PA-12 material behavior.

4 CONCLUSION

This work has investigated the mechanical response of 3D printed PA-12 exposed to tensile loading. Special attention was put on obtaining accurate stress-strain curves over the entire curve up to failure. Issues in accurate and reproducible strain measurements were discovered when relying on extensometer readings for these materials, and it was found that 3D DIC was essential in obtaining good results. Finally, while ASTM standards do not provide fixed strain ranges for determination of Young's modulus, the lack of a true linear region in the case of PA-12 results in significant changes in Young's modulus depending on the used strain range.
The results of the different experiments have revealed 3D printed PA-12 to be an isotropic material regarding its stiffness and Poisson's ratio. With regards to UTS and failure strain, an anisotropic response was observed as a consequence of the layered manufacturing using in the SLS process.
Important stress-relaxation was observed during testing, revealing the visco-elastic material behavior of PA-12. In order to assess the viscous contributions, several hysteresis tests to constant stress levels were performed. The results showed a quick stabilization of the hysteresis loop, indicating the stabilization of the sample (no increase of damage). As such, the hysteresis energy in these loops can be considered to be a result of the viscous nature of PA-12, and can be used to make a first estimate of the viscous nature of PA-12.

ACKNOWLEDGEMENTS

The authors would like to acknowledge the financial support of the Strategic Initiative for Materials (SIM-Flanders) through the M3-AMCAE and the STREAM project.

REFERENCES

Ajoku, U., N. Saleh, N. Hopkinson, R. Hague and P. Erasenthiran (2006). "Investigating mechanical anisotropy and end-of-vector effect in laser-sintered nylon parts." Proceedings of the Institution of Mechanical Engineers Part B-Journal of Engineering Manufacture **220**(7): 1077-1086.
Cooke, W., R. A. Tomlinson, R. Burguete, D. Johns and G. Vanard (2011). "Anisotropy, homogeneity and ageing in an SLS polymer." Rapid Prototyping Journal **17**(4): 269-279.
Goodridge, R. D., C. J. Tuck and R. J. M. Hague (2012). "Laser sintering of polyamides and other polymers." Progress in Materials Science **57**(2): 229-267.
Munguia, J. and K. Dalgarno (2014). "Fatigue behaviour of laser-sintered PA12 specimens under four-point rotating bending." Rapid Prototyping Journal **20**(4): 291-300.
Ramos-Grez, J., A. Amado-Becker, M. J. Yanez, Y. Vargas and L. Gaete (2008). "Elastic tensor stiffness coefficients for SLS Nylon 12 under different degrees of densification as measured by ultrasonic technique." Rapid Prototyping Journal **14**(5): 260-270.
Salazar, A., A. Rico, J. Rodriguez, J. S. Escudero, R. Seltzer and F. M. D. Cutillas (2014). "Monotonic loading and fatigue response of a bio-based polyamide PA11 and a petrol-based polyamide PA12 manufactured by selective laser sintering." European Polymer Journal **59**: 36-45.
Shaffer, S., K. J. Yang, J. Vargas, M. A. Di Prima and W. Voit (2014). "On reducing anisotropy in 3D printed polymers via ionizing radiation." Polymer **55**(23): 5969-5979.
Starr, T. L., T. J. Gornet and J. S. Usher (2011). "The effect of process conditions on mechanical properties of laser-sintered nylon." Rapid Prototyping Journal **17**(6): 418-423.
Van Hooreweder, B., D. Moens, R. Boonen, J. P. Kruth and P. Sas (2013). "On the difference in material structure and fatigue properties of nylon specimens produced by injection molding and selective laser sintering." Polymer Testing **32**(5): 972-981.

Zarringhalam, H., N. Hopkinson, N. F. Kamperman and J. J. de Vlieger (2006). "Effects of processing on microstructure and properties of SLS Nylon 12." Materials Science and Engineering a-Structural Materials Properties Microstructure and Processing **435**: 172-180.